Characterizing synchronization in time series using information measures extracted from symbolic representations

Roberto Monetti,* Wolfram Bunk, and Thomas Aschenbrenner
Max-Planck-Institut für Extraterrestrische Physik, Giessenbachstrasse 1, 85748 Garching, Germany

Ferdinand Jamitzky
Leibniz Supercomputing Centre of the Bavarian Academy of Sciences and Humanities, Boltzmannstrasse 1, 85748 Garching, Germany

(Received 7 November 2007; revised manuscript received 11 November 2008; published 6 April 2009)

We present a methodology to characterize synchronization in time series based on symbolic representations. Each time series is mapped onto a sequence of p-dimensional delay vectors that are subsequently transformed into symbols by means of a rank-ordering of their values. Based on these representations, we propose a transcription scheme between symbols of the respective time series to study synchronization properties. Group-theoretical considerations and the use of information measures allow us to classify regimes of synchronization and to assess its strength. We apply our method to a prototype nonlinear system, which reveals a rich variety of coupled dynamics. We investigate in detail the robustness of the derived synchronization measure against noise and compare its value with that of the established measures.

DOI: 10.1103/PhysRevE.79.046207 PACS number(s): 05.45.Tp, 05.45.Xt

I. INTRODUCTION

Synchronization phenomena are ubiquitous in nature. They take place among coupled oscillatory systems. Synchronization is not restricted to periodic systems; it is also observed in nonlinear chaotic systems. In this case, its emergence is by no means trivial due to the high sensitivity of chaotic systems to initial conditions. Examples of synchronization arise in different fields of science, such as electronics (e.g., coupled circuits), physiology (e.g., spatiotemporal structuring of electroencephalographic signals or between cardiac and respiratory systems) [1,2], extended ecological systems [3], or in nonlinear optics (e.g., coupled laser systems with feedback). Different synchronization states have been identified in the study of coupled chaotic systems, namely complete synchronization [4], phase [5,6] and lag-synchronization [7], generalized synchronization [8,9], etc. (for a review about synchronization in chaotic systems, see [10]).

Here, we present a methodology to characterize synchronization in coupled systems where information measures are obtained using symbolic representations of time series. The methodology is described in Sec. II, where we introduce symbolic representations, the transcription scheme, the concept of order classes and its properties, and the information measures to quantify the degree of synchronization. The application of the method to a coupled chaotic system is presented in Sec. III, and the following subsections discuss different aspects of its dynamics. Special attention is given to the behavior of the probability density of order classes for the different synchronization regimes (Sec. III A) and the analysis of intermittent-lag synchronization (Sec. III C). A comparison of our results with those obtained using well-established synchronization measures is presented in Sec. III B, and Sec. III D is dedicated to an analysis of the robustness of the proposed methodology against Gaussian additive noise.

II. METHOD

Let x be a time series and $q=(x_0,\ldots,x_{p-1})$ be a sequence of length p extracted from x. The symbol Q associated with q is defined as the rank-ordered indices of the components of q. For instance, for $q=(1.6,1.3,1.4,1.5)$, the symbol associated is $Q=(3,0,1,2)$. This symbolic representation was first introduced by Bandt *et al.* [11] in the context of complexity analysis of time series. This approach motivated some studies on the characterization of similarities in time series [12,13]. It should be mentioned that the occurrence of identical values in q has not been considered. When the sequence contains equal values, one can always add a small random perturbation to avoid this case.

Figure 1 shows symbolic representations of two time series (light gray symbols) for $p=4$. Given two symbols A_1 and A_2, there always exists a symbol T, in the following called transcription, such that the composition $T[A_1]=A_2$. The action of symbol T is defined as follows. Let us consider $A_1=(j_0,j_1,\ldots,j_{p-1})$ and $T=(k_0,k_1,\ldots,k_{p-1})$. Then,

$$T[A_1]=(j_{k_0},j_{k_1},\ldots,j_{k_{p-1}}). \tag{1}$$

It should be noted that the set of symbols forms a finite non-Abelian group of order $p!$ with operation T known as the symmetric group S_p. Dark gray symbols in Fig. 1 indicate the transcriptions between the symbolic representations of the time series. The group S_p can be partitioned into nonoverlapping order classes $\mathcal{C}_i$ ($S_p=\cup\mathcal{C}_i$) satisfying a power relation, namely if $T\in\mathcal{C}_N$, then $T^N=I$, where $I=(0,1,\ldots,p-1)$ is the identity symbol and T^N is the composition $T[T^{N-1}]$ with $N\geqslant 1$ and $T^0\equiv I$. Figure 2 (left panel) displays the transcription matrix for $p=3$, where the three existing order classes, i.e., $T=I$ (light gray symbol), $T^2=I$ (black symbols), and $T^3=I$ (dark gray symbols), are shown. It is worth discussing the

*monetti@mpe.mpg.de

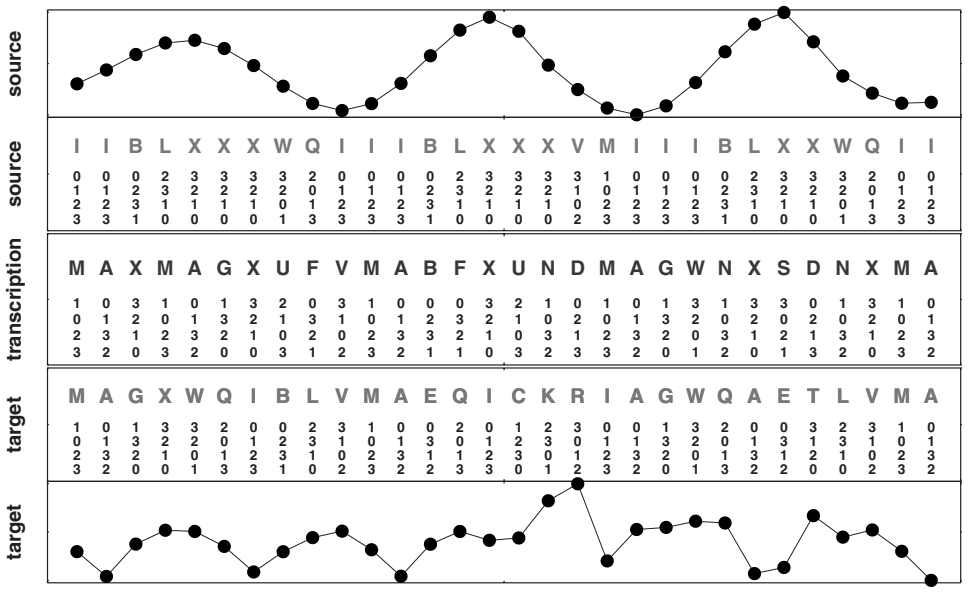

FIG. 1. Example of symbolic representations of time series for sequence length $p=4$. Symbols in light gray correspond to the representations and the dark gray symbols indicate the transcriptions that have to be applied to the upper symbols (source) to obtain the lower ones (target). Note that this operation is not commutative.

action of transcriptions for different order classes. The identity transcription leaves symbols unchanged, thus it is the simplest transcription. For $p=3$, consider transcription $A=(0,2,1)$, which belongs to order 2 class, and apply it to $E=(2,1,0)$ (see Fig. 2),

$$A[E] = D = (2,0,1). \tag{2}$$

Then, the action of A is identical to one transposition, i.e., the interchange of 0 and 1 in symbol E. However, if we consider $B=(1,2,0)$, which belongs to order 3 class, and apply it to $E=(2,1,0)$, the result is $C=(1,0,2)$. We have to perform either two transpositions or one cyclic permutation on E to obtain C. Note that for $p=3$, all order-2 transcriptions cause a one transposition change while all order-3 transcriptions lead to two consecutive transpositions. Thus, we interpret order-3 transcriptions as "more complex" than order-2 transcriptions. In general, the complexity of a transcription T is assessed by a dissimilarity measure between the source and the target symbols given by the minimum number N of recursive applications of T to yield the identity symbol I, i.e., N is the order class of the transcription.

The order classes satisfy an important property of invariance. Let A and B be two symbols connected by the transcription T, i.e., $T[A]=B$, and suppose that $T^N=I$, i.e., $T \in \mathcal{C}_N$. Let Y be an arbitrary transcription such that $Y[A]=C$ and $Y[B]=D$. There always exists a transcription T' such that $T'[C]=D$. We will prove that T' belongs to order-N class as well. In fact,

$$T'[C] = D \Rightarrow T'[Y[A]] = Y[B]. \tag{3}$$

Then,

$$T'[Y[A]] = Y[T[A]]. \tag{4}$$

Applying $A^{-1}Y^{-1}$ on the right to both sides of Eq. (4) and using the associative property of the group, we obtain

$$T' = YTY^{-1}. \tag{5}$$

Since $T \in C_N$, then $T'^N=I$, so T and T' belong to the same order class. This property of invariance also implies that T and T^{-1} belong to the same order class. However, an order class is not a group since it does not satisfy closure. Note that Eq. (5) implies that order classes are also conjugacy classes. Figure 2 (right panel) shows the structure generated by the set C_2 for $p=5$. The symmetry displayed by this structure is a general property found in all order classes since it is a consequence of Eq. (5).

The action of a transcription is just equivalent to applying permutations. It is well known that any permutation can be

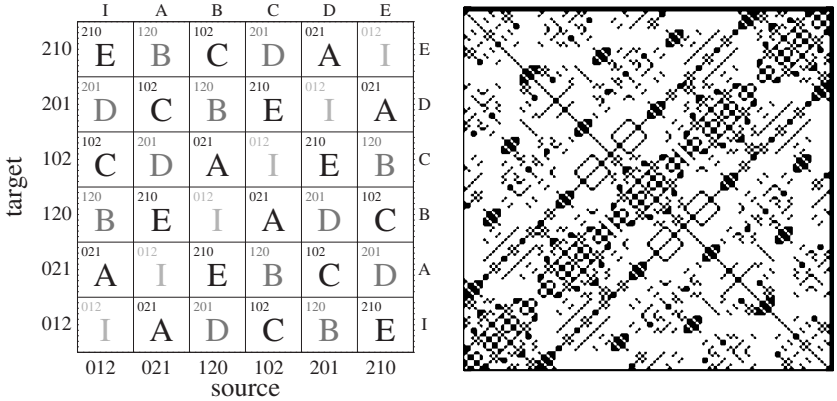

FIG. 2. Left: Transcription matrix for sequence length $p=3$. The black (dark gray) symbols belong to order-2 (-3) class, respectively. The identity symbol (light gray) is a one symbol class satisfying $T^N=I, \forall N$. Right: For $p=5$, the transcription matrix has $(5!)^2$ elements. This matrix shows the positions of the elements belonging to order-2 class, i.e., the structure generated by order-2 transcriptions for $p=5$.

written as a product of disjoint cyclic permutations (DCP). Using this fact, one can prove that the order of any transcription is the least common multiple (LCM) of the lengths of the DCP, where the length of a cyclic permutation is defined as the number its elements. Then, given a sequence length p, one can calculate not only the number of classes but also which orders will be present. In fact, since the sum of the lengths of the DCP equals the sequence length p, the succession of order classes is never interrupted up to order p. For instance, let us consider $p=7$ and calculate the number of classes. As explained above, the identity class and order-2 to -7 classes will be present. Order-8,-9, and -11 classes are missing since there is no possible splitting of a transcription of length 7 in DCP, which shows that the LCM is 8, 9, or 11, respectively. However, order-10 and -12 classes are present since there are transcriptions that can be expressed as a combination of DCP of lengths 2 and 5 for order 10, and 3 and 4 for order 12, respectively. Thus, for $p=7$, nine order classes are present [compare Fig. 4(b)]. Note that for $p \geqslant 7$, classes greater than p and gaps of missing classes always occur.

We now focus on the probability density of transcriptions. Consider a source and a target symbolic representation generated by the actual coupled dynamics of the time series. Given a sequence of length p, the set of all feasible symbols $\mathcal{S}^1=\{X_i\}$ and $\mathcal{S}^2=\{X_j\}$ conforms the state spaces for the source and the target representations, respectively. The probability density of transcriptions $P_T(p)$ can be written as follows:

$$P_{T_k}(p) = \sum_{\Omega=\{(i,j):T_k[X_i]=X_j\}} P^J(X_i,X_j), \tag{6}$$

where $X_i \in \mathcal{S}^1$, $X_j \in \mathcal{S}^2$, and $P^J(X_i,X_j)$ is the joint probability density. Let $P^{(1)}(X_i)$ and $P^{(2)}(X_j)$ be the marginal probability densities of the symbols X_i and X_j in state spaces $\mathcal{S}^1$ and $\mathcal{S}^2$, respectively. The matrix $M_{i,j}=P^{(1)}(X_i)P^{(2)}(X_j)$ is the probability density matrix of transcriptions for two independent processes. In this case, the probability density of transcriptions $P_T^e(p)$ can be evaluated as follows:

$$P^{\text{ind}}_{T_k}(p) = \sum_{\Omega=\{(i,j):T_k[X_i]=X_j\}} M_{i,j}, \tag{7}$$

where $X_i \in \mathcal{S}^1$ and $X_j \in \mathcal{S}^2$. The aim is to find an information measure to assess how much P_T deviates from P_T^{ind}. A natural choice to quantify the contrast between probability densities is the Kullback-Leibler (KL) entropy,

$$E_{\text{KL}}(P,P^{\text{ind}}) = \sum_i P_{T_i}(p)\log_2[P_{T_i}(p)/P^{\text{ind}}_{T_i}(p)]. \tag{8}$$

Since the E_{KL} is not a symmetric quantity, we use the following symmetric form derived via the harmonic mean of $E_{\text{KL}}(P,P^{\text{ind}})$ and $E_{\text{KL}}(P^{\text{ind}},P)$ [14]:

$$S_{\text{KL}}(p) = \frac{E_{\text{KL}}(P,P^{\text{ind}})E_{\text{KL}}(P^{\text{ind}},P)}{E_{\text{KL}}(P,P^{\text{ind}}) + E_{\text{KL}}(P^{\text{ind}},P)}. \tag{9}$$

In contrast to the KL symmetric form, which uses just the arithmetic mean, $S_{\text{KL}}(p)$ satisfies that $S_{\text{KL}}(p) \leqslant \min(E_{\text{KL}}(P,P^{\text{ind}}),E_{\text{KL}}(P^{\text{ind}},P))$ and thus remains always finite. Other properties are discussed in [14].

We demonstrated above that order classes are also conjugacy classes. This important property implies that T and T^{-1} belong to the same order class. Thus, $S_{\text{KL}}(p)$ for transcriptions inside a class is a suitable invariant measure under the interchange of source and target time series. This property of invariance also allows us to calculate the Kullback-Leibler entropy $S^{\mathcal{C}}_{\text{KL}}(p)$ applied to the probability density of order classes $P_{\mathcal{C}}$ (examples of $P_{\mathcal{C}}$ are shown below in Fig. 4). In this case, equations analogous to Eqs. (6)–(9) can easily be derived. In the following, we will refer to S_{KL} obtained using the probability density of transcriptions within a single order class $\mathcal{C}_N$ as $S^N_{\text{KL}}, N=\{2,3,\ldots\}$.

The dynamics of coupled systems may lead to the extinction of order classes. We will refer to this feature as saturation. When saturation occurs, the Kullback-Leibler entropy [Eq. (9)] is not defined. However, for the vanishing order class the probability density of transcriptions for the independent processes P_T^{ind} is nonvanishing. Information theoretical arguments based on the fact that $S_{\text{KL}}(p) \leqslant \min(E_{\text{KL}}(P,P^{\text{ind}}),E_{\text{KL}}(P^{\text{ind}},P))$ suggest that in the route to saturation S^N_{KL} approaches the Shannon information entropy of P_T^{ind}. Thus, in the case of saturation we set $S^N_{\text{KL}}=-\Sigma_i P^{\text{ind}}_{T_i}\log_2 P^{\text{ind}}_{T_i}$.

It should be emphasized that $S_{\text{KL}}(p)$ quantifies the deviation of the coupled dynamics with respect to that of independent processes that conserve the probability density of the symbolic representations.

III. APPLICATIONS

We apply the method to a bidirectionally coupled Roessler-Roessler system [7] defined by the following set of equations:

$$\begin{aligned}
\dot{x}_{1,2} &= -w_{1,2}y_{1,2} - z_{1,2} + k(x_{2,1} - x_{1,2}),\\
\dot{y}_{1,2} &= w_{1,2}x_{1,2} + 0.165y_{1,2},\\
\dot{z}_{1,2} &= 0.2 + z_{1,2}(x_{1,2} - 10),
\end{aligned} \tag{10}$$

where $w_1=0.99$ and $w_2=0.95$ are the mismatch parameters. All time series were generated using a fourth-order Runge-Kutta method with an increment $\delta t=0.001$ and the following initial conditions: $x_1(0)=-0.4$, $y_1(0)=0.6$, $z_1(0)=5.8$, $x_2(0)=0.8$, $y_2(0)=-2$, and $z_1(0)=-4$. Results were saved at intervals $\Delta t=0.01$. This chaotic system exhibits a rich synchronization behavior which ranges from phase ($k \approx 0.036$) to lag ($k \approx 0.14$) and finally to complete synchronization as the coupling parameter k is increased [7]. The results presented here were obtained using the x components of the Roessler subsystems. For every time series, we generate p-dimensional delay vectors $\vec{v}_i=(x(t_i),x(t_{i+\tau}),\ldots,x(t_{i+(p-1)\tau}))$ $(i=\{0,1,\ldots,L-1-\tau(p-1)\})$. A symbolic representation is obtained by transforming the sequence of delay vectors into symbols. We considered time series of length $L=2^{19}$ ($\sim$775 orbits) and a delay $\tau=150\Delta t$, which fulfills the condition of minimum mutual information of the delay coordinates $(x_1(t),x_1(t+\tau))$ for the uncoupled system $(k=0)$ [15]. Using these settings, we expect a higher

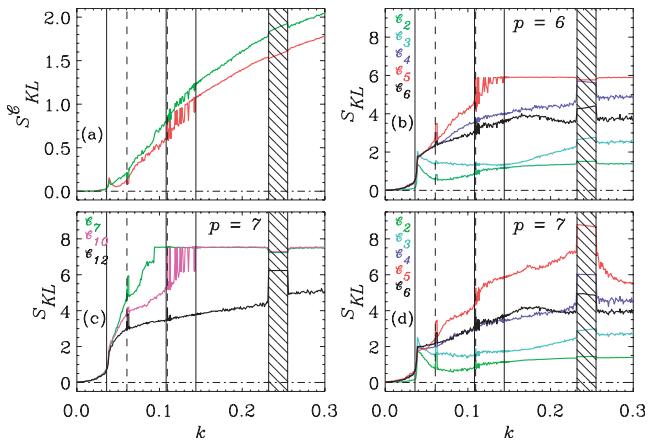

FIG. 3. (Color) (a) $S_{\mathrm{KL}}^{\mathcal{C}}$ obtained using the probability density of order classes for $p=6$ (red curve) and $p=7$ (green curve). (b), (c), (d) Kullback-Leibler entropy S_{KL} obtained using the probability density of transcriptions for the order classes and sequence lengths indicated in the plots. Vertical full lines from left to right indicate transitions to phase synchronization ($k\sim0.036$), intermittent-lag synchronization ($k\sim0.11$), and lag synchronization ($k\sim0.145$), respectively. Vertical dashed lines at $k\sim0.061$ and $k\sim0.11$, and hatched areas ($k\in[0.232,0.256]$) indicate periodic windows. The values of the coupling constant for the onset of phase synchronization and the first periodic window were taken from [7].

response of our measures to the influence of the coupling.

Figure 3(a) shows the Kullback-Leibler entropy $S_{\mathrm{KL}}^{\mathcal{C}}$ obtained using the probability density of order classes $P_{\mathcal{C}}$ for $p=6$ and 7. Figures 3(b)–3(d) show S_{KL} obtained using the probability density of transcriptions in all feasible order classes for $p=6$ and 7. We first discuss the behavior of the coupled system using the results for $S_{\mathrm{KL}}^{\mathcal{C}}$. For small values of the coupling constant k, the time series behave independently since the Roessler subsystems are almost uncoupled. For $k\in[0,0.036]$, $S_{\mathrm{KL}}^{\mathcal{C}}$ indicates that the actual dynamics hardly deviates from that of the independent processes. $S_{\mathrm{KL}}^{\mathcal{C}}$ increases at $k\sim0.036$ due to the transition to phase synchronization. For stronger coupling k, $S_{\mathrm{KL}}^{\mathcal{C}}$ increases again rather monotonically until $k\sim0.11$. For $k\in[0.11,0.145]$, $S_{\mathrm{KL}}^{\mathcal{C}}$ displays strong fluctuations revealing the presence of "intermittent-lag synchronization." This particular synchronization regime characterized by synchronization periods interrupted by bursts of nonsynchronized activity [7,16] is discussed in detail in the following sections. The strong fluctuations displayed by $S_{\mathrm{KL}}^{\mathcal{C}}$ sharply vanish at the onset of lag synchronization ($k\sim0.145$). Lag synchronization is defined through the condition $x_1(t+\tau_0)=x_2(t)$, i.e., the coincidence of the time series when shifted in time by a constant time lag τ_0. Curves increase monotonically in the interval $k\in[0.145,0.30]$ reflecting stronger synchronization. This trend is only interrupted within the coupling range $k\in[0.232,0.256]$ where a period-5 window occurs.

The periodic windows are better observed in Figs. 3(b)–3(d). In fact, all curves display a peak at $k\approx0.061$ that corresponds to a period-3 window [7]. S_{KL}^{6} for $(p=6)$ and S_{KL}^{12} for $(p=7)$ indicate a period-6 window at $k\approx0.11$. To the best of our knowledge, the existence of this periodic window has not been reported before, probably due to its extremely small size ($k\in[0.1094,0.1096]$). All curves show signatures (some of them are strong) of the occurrence of periodic behavior within the coupling range $k\in[0.232,0.256]$. Intermittent-lag synchronization is particularly reflected by the strong fluctuations observed in Figs. 3(b) and 3(c) for S_{KL}^{5} for $(p=6)$ and S_{KL}^{10} for $(p=7)$, which sharply vanish at $k=0.145$.

Figure 3 also reveals that the Kullback-Leibler entropy of some high-order classes saturates when increasing the values of the coupling constant k. In fact, Figs. 3(b) and 3(c) show that the coupled dynamics lead to the extinction of order classes $\mathcal{C}^5$ for $(p=6)$, $\mathcal{C}^7$ for $(p=7)$, and $\mathcal{C}^{10}$ for $(p=7)$ at $k\sim0.145$, $k\sim0.09$, and $k\sim0.145$, respectively.

It should be mentioned that certain order classes are better suited for describing a particular feature of the system than others. For instance, for $p=6$, S_{KL}^{5} characterizes the intermittent-lag synchronization behavior and the onset of lag synchronization better than S_{KL}^{6}. In this sense, different order classes provide complementary information of the coupled system.

A. The behavior of order classes for different synchronization regimes

Figures 4(a) and 4(b) show the probability density $P_{\mathcal{C}_i}$ of the order classes for $p=6$ and 7, respectively. Note that Fig. 3(a) displays the contrast between probability densities as in Fig. 4 and those of the independent processes. Figure 3(a) indicates that for $k=0.005$ the contrast is vanishing ($S_{\mathrm{KL}}^{\mathcal{C}}\sim0$). This result is in agreement with the behavior of the Roessler subsystems observed for the same value of the coupling constant. A vanishing contrast implies that the probability density $P_{\mathcal{C}}$ for $k=0.005$, which is clearly nonuniform, is similar to that generated by two independent processes. Note that even for two random independent processes, the probability density of order classes is not uniform since the cardinality of order classes is different. In the vicinity of the transition to phase synchronization, $P_{\mathcal{C}}$ deviates from that of the independent processes [see Fig. 3(a)] and higher-order classes dominate the coupled dynamics [see Figs. 4(a) and 4(b) for $k=0.039$]. This trend is reversed with increasing k, and already at $k=0.062$ $(k=0.074)$ for $p=6$ $(p=7)$ $\mathcal{C}_2$ is the most relevant class. Figure 4(a) shows that $\mathcal{C}_2$ dominates up to large values of k where finally $\mathcal{C}_I$ prevails. Figure 4(b) reveals the same trends as in (a) except that $\mathcal{C}_2$ still dominates at $k=0.299$.

We discussed above the different synchronization regimes displayed by the coupled Roessler system that occur in the range $k\in[0,0.30]$. Phase synchronization, which arises at $k\sim0.036$, is defined by a phase-locking condition between the subsystems while the amplitudes may remain chaotic and uncorrelated [5]. For increasing coupling values, stronger synchronization regimes arise, e.g., lag synchronization, where not only a phase-locking condition is fulfilled but the amplitudes become correlated. In this sense, phase synchronization is the weakest form of synchronization displayed by this system. At the same time, the fact that for phase synchronization amplitudes remain chaotic and uncorrelated imposes a more "complex" relationship between the sub-

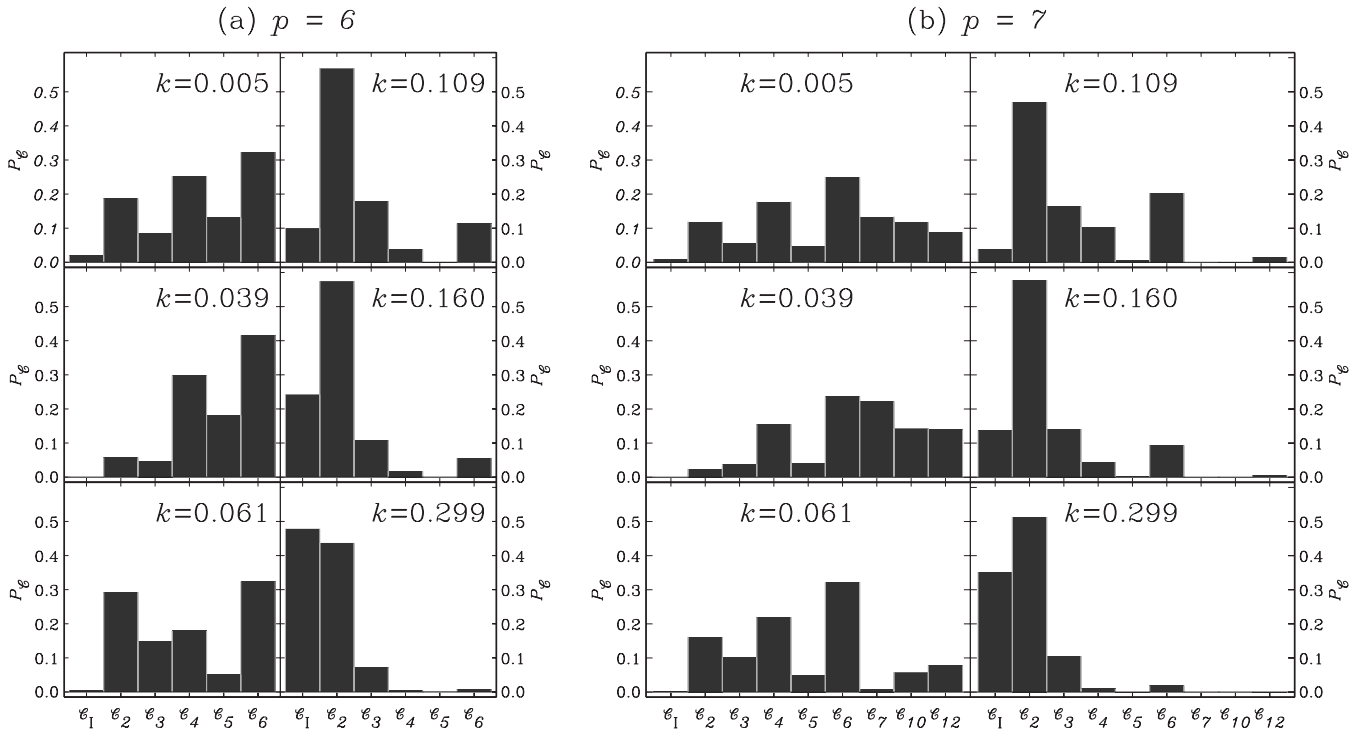

FIG. 4. (a) Probability density P_C of the existing order classes for different values of the coupling constant k for $p=6$. Note that class $\mathcal{C}_I$ comprises only the identity $I=(0,1,2,3,4,5)$. (b) Idem (a) for $p=7$. Order-8, -9, and -11 classes are not allowed.

systems than that for other synchronization regimes. For instance, for lag or complete synchronization the amplitudes are related via $x_1(t)=x_2(t+\tau)$ with $\tau\neq 0$ or $\tau=0$, respectively. Consequently, while stronger synchronization regimes arise for increasing values of the coupling constant k, the relationship between the synchronized subsystems becomes simpler.

We have argued above that the order of a transcription estimates its "complexity." Thus, the probability density of order classes indicates how "complex" the relationship between the time series is. Figure 4 demonstrates that higher-order transcriptions play an important role in the description of complex synchronization states such as phase synchronization ($k\gtrsim 0.036$). For increasing k, the probability densities of higher-order classes decrease and some of them vanish, such as $\mathcal{C}_5$ for $p=6$ and $\mathcal{C}_7$ and $\mathcal{C}_{10}$ for $p=7$. In fact, simpler synchronization states such as intermittent lag and lag synchronization ($k>0.11$) are predominantly described by lower-order classes ($\mathcal{C}_2$ and $\mathcal{C}_I$). Clearly, the simplest synchronization state, namely complete synchronization, will only be described by the identity ($\mathcal{C}_I$).

B. Comparison with other synchronization measures

Here, we compare our methodology with two well-established approaches to characterize synchronization.

The concept of instantaneous phase $\phi(t)$ of a signal, originally introduced by Gabor [17], is based on the Hilbert transform and was brought into the context of chaotic synchronization by Rosenblum *et al.* [5]. Here, we do not consider the Hilbert phases or phase differences as monotonically increasing quantities as in [2]. We use instead the phases defined in the interval $]-\pi,\pi]$ and calculate the mutual information I_ϕ to quantify the strength of synchronization [18]. The mutual information I_ϕ is defined as follows:

$$I_\phi = \int_{-\pi}^{\pi}\int_{-\pi}^{\pi} D(\phi_1,\phi_2)\log_2\frac{D(\phi_1,\phi_2)}{D_1(\phi_1)D_2(\phi_2)}d\phi_1 d\phi_2, \tag{11}$$

where $D(\phi_1,\phi_2)$ is the joint probability distribution of the Hilbert phase variables and $D_1(\phi_1)$ and $D_2(\phi_2)$ are the marginal probability distributions for each of the phase variables.

We have also considered the similarity function S introduced in [7], defined as the time-averaged difference between the variables x_1' and x_2' ($\langle x_1'\rangle=0$, $\langle x_2'\rangle=0$) taken with a time shift τ,

$$S^2(\tau) = \frac{\langle[x_1'(t)-x_2'(t-\tau)]^2\rangle}{[\langle x_1'^2(t)\rangle\langle x_2'^2(t)\rangle]^{1/2}}, \tag{12}$$

and search for its minimum $\sigma=\min_\tau S(\tau)$. For signals having the same standard deviation, $S(\tau')=\sqrt{2}$ for all τ' if the signals are independent. For lag or completely synchronized signals, $S(\tau')=0$ with $\tau'\neq 0$ or $\tau'=0$, respectively.

Figure 5 shows the behavior of the well-established synchronization measures as a function of the coupling constant k. For the sake of comparison, $S_{\mathrm{KL}}^{\mathcal{C}}$ for $p=6,7$ has also been included. The mutual information I_ϕ is able to differentiate between unsynchronized and phase-synchronized behavior since it sharply increases at $k\sim 0.036$. However, for $k=0$, I_ϕ indicates a counterintuitive nonvanishing synchronization level that was not observed for other synchronization measures. For the range $k\in[0.04,0.11]$, I_ϕ increases and shows local maxima at the position of the period-3 window (k

~ 0.061) and at the position of the period-6 window ($k \sim 0.11$). For $k \gtrsim 0.11$, the mutual information I_ϕ displays strong fluctuations that quickly become weaker and disappear for $k > 0.13$. In the range $k \in [0.13, 0.30]$, a rather monotonically increasing behavior is observed only interrupted by a step in the range $k \in [0.232, 0.256]$, which indicates the presence of periodic windows.

We observe that for $k=0$, $\sigma = \sqrt{2}$ and it decreases for increasing values of the coupling constant. At $k \sim 0.036$, σ sharply changes its local slope indicating the transition to phase synchronization. σ displays an outburst at $k \sim 0.061$, where a period-3 window is observed [7], and decreases for further increasing k until it vanishes at $k \sim 0.145$, indicating the onset of lag synchronization. For $k > 0.145$, $\sigma = 0$ and thus provides no further information about the dynamics of the coupled system.

We conclude that σ and I_ϕ are suitable quantities that correctly characterize most of the features of this coupled system, such as the onset of phase synchronization and the presence of periodic windows. As expected, σ provides an accurate estimate of the onset of lag synchronization but is not sensitive to the stronger synchronization level that takes place for increasing values of the coupling constant k. In contrast, for $k \in [0.13, 0.30]$, I_ϕ displays an increasing behavior indicating stronger synchronization but it fails to estimate accurately the onset of lag synchronization. The proposed synchronization measures are able to characterize all the features of these coupled systems. This comparative study indicates that the intermittent-lag-synchronization behavior and the onset of lag synchronization are best characterized by our synchronization measures.

C. The intermittent-lag-synchronization

As mentioned above, for $k \in [0.11, 0.145]$, the coupled system displays a typical behavior known as intermittent-lag synchronization, characterized by synchronization periods interrupted by bursts of nonsynchronized behavior. Figure 3 shows that within this range of k values, S_{KL} displays fluctuations that are particularly strong for S_{KL}^5 ($p=6$) [see Fig. 3(b)] and S_{KL}^{10} ($p=7$) [see Fig. 3(c)], and for $S_{\mathrm{KL}}^{\mathcal{C}}$ [see Fig. 3(a)], and vanish for $k > 0.145$. In order to investigate if the observed fluctuations are related to this particular synchronization state, we considered time series where intermittent-lag synchronization occurs as shown in the upper panel of Fig. 6. Using these time series, we performed a sliding window analysis and calculated the Kullback-Leibler entropy S_{KL}^2 and $S_{\mathrm{KL}}^{\mathcal{C}}$ for $p=6$ and 7. For the sake of comparison, we also show the behavior of the mutual information I_ϕ. Here, we have considered S_{KL}^2 instead of the Kullback-Leibler entropy for the order classes S_{KL}^5 ($p=6$) or S_{KL}^{10} ($p=7$), which displayed the highest response to this synchronization regime in a global analysis. The reason for this choice was to investigate if the dominant order class ($\mathcal{C}_2$) in this range of coupling values ($k \in [0.11, 0.145]$)—although unable to clearly unveil intermittent-lag synchronization in a global analysis—is sensitive to the details of the coupled dynamics when using a sliding window analysis.

The third and fourth panels of Fig. 6 show that S_{KL}^2 and $S_{\mathrm{KL}}^{\mathcal{C}}$ display dips when bursts of nonsynchronized activity occur and high values (peaks) during synchronized periods. The second panel of Fig. 6 shows that I_ϕ displays a similar behavior, thus providing a good description of this particular synchronization state. It should be noted, however, that the contrast between synchronized and nonsynchronized periods is rather enhanced when applying our proposed synchronization measures.

Let us focus again on the global analysis of the system shown in Figs. 3 and 5. The results obtained using the sliding window analysis suggest that fluctuations displayed by $S_{\mathrm{KL}}^{\mathcal{C}}$ and S_{KL} for $k \in [0.11, 0.145]$ are due to the intermittent-lag-synchronization behavior. Bursts of nonsynchronized activity become less frequent when the coupling constant approaches the value $k=0.145$ where they vanish. This value of the coupling constant is in agreement with the one reported in [7] for the onset of lag synchronization. We also found that the presence of transcriptions in $\mathcal{C}_5$ ($p=6$) and $\mathcal{C}_{10}$ ($p=7$) is highly correlated with the presence of bursts of nonsynchronized activity. In fact, during synchronized periods, the number of transcriptions in these classes (not shown here) strongly decreases or even vanishes, thus leading to the strong fluctuations observed in S_{KL}^5, S_{KL}^{10}, and $S_{\mathrm{KL}}^{\mathcal{C}}$. Figure 5 shows that I_ϕ does not display particularly strong fluctuations in the whole interval $k \in [0.11, 0.145]$, although the sliding window study indicated that I_ϕ was able to unveil the details of the synchronization dynamics. Thus, I_ϕ is not so sensitive to the intermittent-lag-synchronization behavior as the new information measures derived from some particular order classes. Note that σ also displays small fluctuations for $k \in [0.11, 0.145]$ (see Fig. 5), which are due to bursts of nonsynchronized activity.

Finally, this sliding window approach demonstrates the reliability of our method even for shorter time series.

D. The influence of noise

We have also applied our method to the coupled Roessler system in the presence of superimposed additive white Gaussian noise with varying standard deviations Σ_n. The signal-to-noise ratio (SNR) is defined as $X_{\mathrm{SNR}} = \Sigma_s / \Sigma_n$, where Σ_s is the standard deviation of the original time series. We have considered as before the x components of the Roessler subsystems and added white Gaussian noise independently to both components. We first perform a detailed analysis to assess which of the new information measures derived from the symbolic transcription scheme is more robust against additive Gaussian noise. Then, we present a comparative analysis including the behavior of σ and I_ϕ for the noisy time series.

Figure 7 shows the behavior of four different order classes for $X_{\mathrm{SNR}} = \{16, 8, 4, 2\}$. All quantities are sensitive to different SNR values and show the expected trend, i.e., they decrease for decreasing SNR values. They also indicate clearly the onset of phase synchronization for all SNR values considered here. Figure 7(a) shows the Kullback-Leibler entropy $S_{\mathrm{KL}}^{\mathcal{C}}$ obtained using the probability density of order classes. For $X_{\mathrm{SNR}} = 16$, the behavior of $S_{\mathrm{KL}}^{\mathcal{C}}$ is close to the noise-free case (black curve) but strong fluctuations are observed for $k > 0.14$ since noise randomly generates transcriptions of

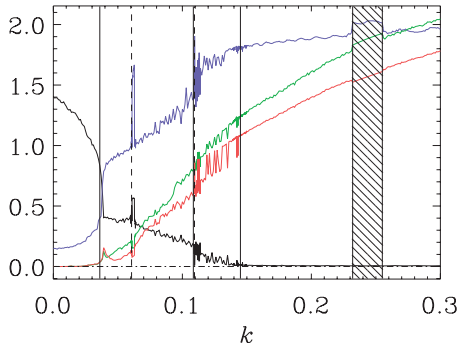

FIG. 5. (Color) Different synchronization measures the coupling constant k. Similarity measure σ (black curve), mutual information I_ϕ (violet curve), $S^{\mathcal{C}}_{\mathrm{KL}}(p=6)$ (red curve), and $S^{\mathcal{C}}_{\mathrm{KL}}(p=7)$ (green curve). I_ϕ was calculated using 512 bins and the resulting curve was scaled by a factor 0.27 in order to fit the range of the other quantities shown in this plot.

classes $\mathcal{C}_7$ and $\mathcal{C}_{10}$, i.e., the classes suppressed by the dynamics of the noise-free coupled system. For lower SNR values, all curves still display an increasing monotonic behavior in the range $k \in [0.04, 0.30]$ indicating stronger synchronization. Figures 7(b)–7(d) show the behavior of the Kullback-Leibler entropy S^2_{KL}, S^3_{KL}, and S^4_{KL}, respectively. Figures 7(c) and 7(d) show that for $X_{\mathrm{SNR}} < 16$, S^3_{KL} and S^4_{KL} are not able to unveil the stronger synchronization for larger values of k since a constant or even a decreasing behavior is observed. In contrast, S^2_{KL} displays an increasing behavior for all SNR values. Thus, we identify $S^{\mathcal{C}}_{\mathrm{KL}}$ and S^2_{KL} as the most robust measures against additive Gaussian noise

We include for the sake of comparison Fig. 8, in which σ, I_ϕ, and $S^{\mathcal{C}}_{\mathrm{KL}}$ versus the coupling constant k for different values of SNR are shown. We observe in all cases the expected trend for decreasing SNR values, i.e., I_ϕ and $S^{\mathcal{C}}_{\mathrm{KL}}$ decrease

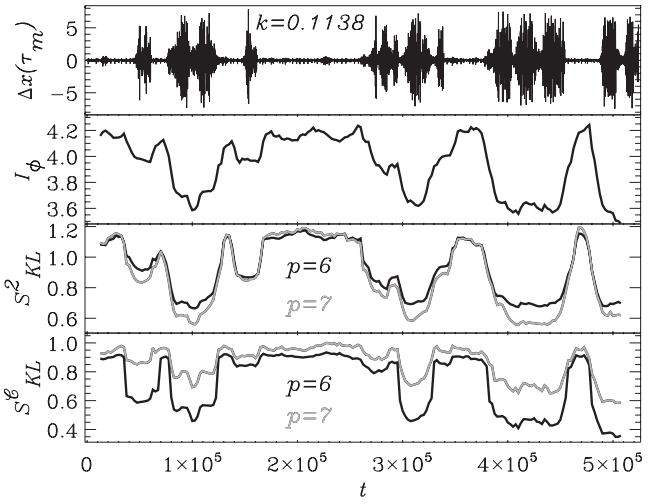

FIG. 6. Upper panel: Difference between the x components of the Roessler subsystems $\Delta x(\tau_m)$ for the time delay $\tau_m = 38$, which satisfies $\min_\tau S(\tau) = S(\tau_m)$. The intermittent bursts of nonsynchronized activity are clearly observed. Second panel: I_ϕ vs t. Third panel: Kullback-Leibler entropy S^2_{KL} for $p=6$ and 7 vs t. Lower panel: $S^{\mathcal{C}}_{\mathrm{KL}}$ for $p=6$ and 7 vs t. Results were obtained using a sliding window analysis for window size $w = 25\,000$.

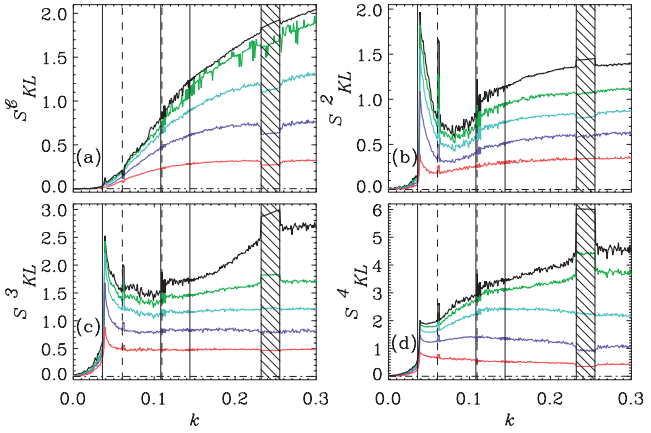

FIG. 7. (Color) (a) $S^{\mathcal{C}}_{\mathrm{KL}}$ vs k for different SNR values. (b) S^2_{KL} vs k for different SNR values. (c) S^3_{KL} vs k for different SNR values. (d) S^4_{KL} vs k for different SNR values. Vertical full lines from left to right indicate transitions to phase, intermittent-lag, and lag synchronization, respectively. Vertical dashed lines and hatched areas indicate periodic windows. Different colors indicate SNRs of 16 (green curves), 8 (blue curves), 4 (violet curves), and 2 (red curves). All results were obtained for sequence length $p=7$.

and σ increases. The transition to the phase-synchronized regime is well described by all synchronization measures for all values of SNR considered here. However, for large values of k the mutual information I_ϕ approaches a constant value, thus being unable to show the stronger synchronization level that persists even in the presence of noise. Signatures of the intermittent-lag-synchronization state are not observed anymore using this global analysis.

For $k > 0.14$, σ also displays an asymptotic constant behavior that can be derived analytically. Let us assume that the standard deviation Σ_s is identical for the two time series $x_1(t)$ and $x_2(t)$ (this is a good approximation for the Roessler system studied here). As mentioned above, for $k > 0.14$ the coupled system displays lag synchronization, thus there ex-

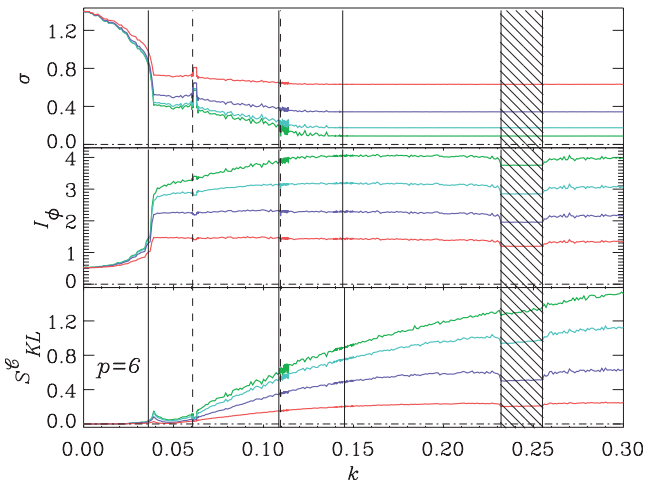

FIG. 8. (Color) Upper panel: Similarity measure σ vs the coupling constant k for different values of SNR. Central panel: I_ϕ vs the coupling constant k for different values of SNR. Lower panel: $S^{\mathcal{C}}_{\mathrm{KL}}$ for $p=6$ vs k. Different colors indicate SNRs of 16 (green curves), 8 (blue curves), 4 (violet curves), and 2 (red curves).

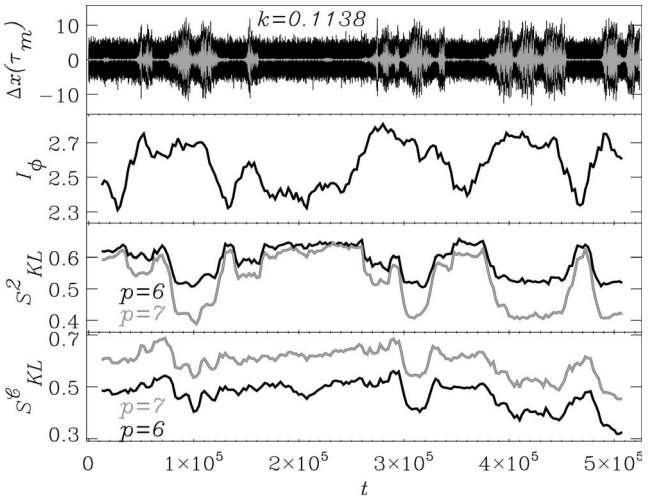

FIG. 9. Upper panel: Difference between the x components of the Roessler subsystems $\Delta x(\tau_m)$ for $X_{\mathrm{SNR}}=6$ (black curve) and time delay $\tau_m=38$. For the sake of reference, we also show the difference between the x components in the absence of noise (light gray curve; see also the first panel of Fig. 6). Second panel: I_ϕ vs t. Third panel: Kullback-Leibler entropy S^2_{KL} for $p=6$ and 7 vs t. Lower panel: $S^{\mathcal{C}}_{\mathrm{KL}}$ for $p=6$ and 7 vs t. Results were obtained using a sliding window analysis for window size $w=25\,000$.

ists a time delay τ' such as $x_2(t+\tau')-x_1(t)=0$. In the presence of noise, the time series can be written as

$$x'_{1,2}(t) = x_{1,2}(t) + \eta_{1,2}(t). \tag{13}$$

Then, it can be shown that within the lag-synchronization regime, σ behaves as

$$\sigma = \sqrt{\frac{2}{1+X^2_{\mathrm{SNR}}}}. \tag{14}$$

As mentioned above, additive noise destroys all signatures of intermittent-lag synchronization when performing a global analysis of the system. We have also investigated whether a sliding window analysis is able to provide any signature of the behavior of the system in the absence of noise. The upper panel of Fig. 9 shows the difference of the x components of the Roessler subsystems for the same coupling value used in Fig. 6 and $X_{\mathrm{SNR}}=6$. For the sake of reference, we have overplotted in light gray the difference of the x components in the absence of noise where the bursts of nonsynchronized behavior are clearly observed. A comparison of the second panels of Figs. 9 and 6 indicates that the noise perturbation has a strong influence on the mutual information of the Hilbert phases I_ϕ. In fact, we observe that I_ϕ displays a counterintuitive behavior opposite to that found in the absence of noise. In contrast, S^2_{KL} (third panel of Fig. 9) reveals exactly the same trend as in the noise-free system. Thus, S^2_{KL} is still able to differentiate between these two synchronization levels in the presence of noise. A comparison of the third panels of Figs. 9 and 6 shows that the curves behave similarly but the amplitude range is smaller. However, S^2_{KL} provides for $p=7$ a better description of the dynamics of the system than for $p=6$ since it displays a higher contrast between the two synchronization levels. $S^{\mathcal{C}}_{\mathrm{KL}}$ behaves also accordingly to the presence or absence of bursts of nonsynchronized behavior, but the sensitivity is lower than that for S^2_{KL}. We have investigated the behavior of all above-mentioned quantities for other SNR values. Our results (not shown here) indicate that I_ϕ is unable to account for differences in the synchronization level of the signals for $X_{\mathrm{SNR}} \leqslant 12$.

We conclude that information measures extracted from symbolic representations, in particular S^2_{KL}, are better suited than I_ϕ to describe the behavior of the coupled system in the presence of noise.

IV. CONCLUSIONS

We presented a method to characterize similarities between time series based on symbolic representations, which is particularly useful to study synchronization. The property of invariance with respect to the interchange of source and target symbolic representations allows us to derive synchronization measures for the different order classes. We demonstrated that different order classes provide complementary information of the synchronization dynamics. We presented a comparative study of our methodology with other well-established approaches to characterize synchronization. Information measures extracted from the newly proposed symbolic transcription scheme proved to be more robust than the other synchronization measures against additive Gaussian noise and offer higher detection sensitivity for particular dynamical features.

The understanding of the action of transcriptions belonging to specific order classes led us to interpret the probability density of order classes as an expression of the "complexity" of the relationship between the coupled systems in terms of the transcription effort. The probability density of order classes shows that more complex synchronization states are mainly described by higher-order classes while lower-order classes dominate for simpler synchronization states. Our approach to characterize synchronization in time series provides a framework in which group-theoretical considerations and information measures can be applied to classify regimes of synchronization and to assess its strength. Our method is also suitable to investigate the behavior of spatially extended systems such as coupled-map lattices or cellular automata. These models, which are able to display complex spatiotemporal dynamics, have been used to describe a wide range of systems such as biological and ecological networks. In particular, we expect our methodology to be useful for the diagnosis of brain activity using multichannel electroencephalographic recordings, where the occurrence of synchronization phenomena plays a relevant role.

[1] C. Schafer, M. Rosenblum, J. Kurths, and H. Abel, Nature **392**, 239 (1998).
[2] P. Tass, M. G. Rosenblum, J. Weule, J. Kurths, A. Pikovsky, J. Volkmann, A. Schnitzler, and H. J. Freund, Phys. Rev. Lett. **81**, 3291 (1998).
[3] B. Blasius, A. Huppert, and L. Stone, Nature **399**, 354 (1999).
[4] L. M. Pecora and T. L. Carroll, Phys. Rev. Lett. **64**, 821 (1990).
[5] M. G. Rosenblum, A. S. Pikovsky, and J. Kurths, Phys. Rev. Lett. **76**, 1804 (1996).
[6] E. Rosa, E. Ott, and M. H. Hess, Phys. Rev. Lett. **80**, 1642 (1998).
[7] M. G. Rosenblum, A. S. Pikovsky, and J. Kurths, Phys. Rev. Lett. **78**, 4193 (1997).
[8] N. F. Rulkov, M. M. Sushchik, L. S. Tsimring, and H. D. I. Abarbanel, Phys. Rev. E **51**, 980 (1995).
[9] L. Kocarev and U. Parlitz, Phys. Rev. Lett. **76**, 1816 (1996).
[10] S. Boccaletti, J. Kurths, G. Osipov, D. Valladares, and C. Zhou, Phys. Rep. **366**, 1 (2002).
[11] C. Bandt and B. Pompe, Phys. Rev. Lett. **88**, 174102 (2002).
[12] Z. Liu, Europhys. Lett. **68**, 19 (2004).
[13] K. Keller and K. Wittfeld, Int. J. Bifurcation Chaos Appl. Sci. Eng. **14**, 693 (2004).
[14] D. Johnson and S. Sinanović, Available from http://citeseer.ist.psu.edu/johnson01symmetrizing.html (2001).
[15] A. M. Fraser and H. L. Swinney, Phys. Rev. A **33**, 1134 (1986).
[16] S. Boccaletti and D. L. Valladares, Phys. Rev. E **62**, 7497 (2000).
[17] D. Gabor, J. IEE London **93**, 429 (1946).
[18] M. Palus, Phys. Lett. A **235**, 341 (1997).